Journal of Controlled Release 335 (2021) 237–246

Contents lists available at ScienceDirect

Journal of Controlled Release

journal homepage: www.elsevier.com/locate/jconrel

Impact of lipid nanoparticle size on mRNA vaccine immunogenicity

Kimberly J. Hassett [1], Jaclyn Higgins [1], Angela Woods, Becca Levy [2], Yan Xia, Chiaowen Joyce Hsiao, Edward Acosta, Örn Almarsson [3], Melissa J. Moore, Luis A. Brito [*]

Moderna, Inc, 200 Technology Square, Cambridge, MA 02139, United States of America

ARTICLE INFO

Keywords:
Vaccine
Nanoparticle
mRNA
Size
Lipid

ABSTRACT

Lipid nanoparticles (LNP) are effective delivery vehicles for messenger RNA (mRNA) and have shown promise for vaccine applications. Yet there are no published reports detailing how LNP biophysical properties can impact vaccine performance. In our hands, a retrospective analysis of mRNA LNP vaccine in vivo studies revealed a relationship between LNP particle size and immunogenicity in mice using LNPs of various compositions. To further investigate this, we designed a series of studies to systematically change LNP particle size without altering lipid composition and evaluated biophysical properties and immunogenicity of the resulting LNPs. While small diameter LNPs were substantially less immunogenic in mice, all particle sizes tested yielded a robust immune response in non-human primates (NHP).

1. Introduction

Vaccines are widely considered one of the greatest public health achievements of the 20th century, saving millions of lives each year through management and eradication of infectious diseases [1,2]. Although licensed vaccines are now available against 30 different pathogens [2], there are still many existing diseases with no vaccine. Pathogen complexity, safety limitations, and manufacturing challenges have rendered traditional vaccine approaches unsuccessful against high priority targets such as respiratory syncytial virus (RSV) and cytomegalovirus (CMV) [1,3–5]. Furthermore, numerous novel pathogens emerge every year – it is estimated that 85 infectious viral diseases emerged between 1940 and 2004, most often originating in wildlife and crossing species at the animal-human interface [6,7]. Recent examples of human diseases with zoonotic origins include acquired immunodeficiency syndrome (AIDS), Ebola, pandemic influenza A and severe acute respiratory syndromes (SARS, COVID-19) [7–10]. As human activity continues to disrupt ecological niches, zoonotic infectious agents will inevitably evolve in response and adapt to enter human populations — increasing the risk for more pandemics [6,7]. New vaccine technologies are therefore needed to both address unmet medical needs and enable rapid development of vaccines against emerging pathogens.

Messenger RNA (mRNA) vaccines are uniquely positioned to address both challenges. Delivery of mRNAs encoding viral antigens allows for antigen production in situ, closely resembling a natural infection with no potential for disease [11,12]. Using this approach, a new vaccine can be made as soon as the antigen sequence is identified. Our SARS-CoV-2 vaccine was manufactured and delivered to clinical sites within 45 days of the viral genome being sequenced and released [13,14]. mRNA vaccines also enable production of complex antigens, including intracellular or transmembrane targets. Further, the expression of multiple antigens or assembly of complex multimeric antigens can be achieved by combining different mRNA sequences in a single immunization [5,12].

Effective mRNA vaccines require both mRNA delivery and antigen expression to enable antigen-specific immunity [15]. Lipid nanoparticles (LNPs) are the leading technology for facilitating intracellular mRNA delivery [5,12,15–21]. LNPs are typically composed of an ionizable lipid, a phospholipid, a sterol, and a lipid-anchored polyethylene-glycol (PEG), with the ionizable lipid being most important for mRNA expression [12,15,22,23]. To date, LNP optimization for mRNA delivery has primarily focused on lipid composition [12,16,22]. We recently published a screen optimizing biodegradable ionizable lipids for intramuscular administration of mRNA vaccines [12]. In that report, we showed that protein expression is not the sole determinant of vaccine potency, indicating that additional factors contribute. With other vaccine technologies, nanoparticle biophysical properties are known to

* Corresponding author.
E-mail address: Luis.Brito@Modernatx.com (L.A. Brito).
[1] Co-first authors.
[2] Present address: Rheos Medicines, 245 First St Suite 200, Cambridge, MA 02142, United States of America.
[3] Present address: Lyndra Therapeutics, 65 Grove St Suite 301, Watertown, MA 02472, United States of America.

https://doi.org/10.1016/j.jconrel.2021.05.021
Received 18 February 2021; Received in revised form 14 May 2021; Accepted 16 May 2021
Available online 18 May 2021

affect immunogenicity. When used as nanocarriers for protein-based vaccines, nanoparticle size impacts innate immune stimulation and nanoparticle tissue and cellular distribution [24–27]. To date, the literature describing the role of vaccine particle size on immunogenicity has solely focused on protein antigens with particulate adjuvants for innate immune stimulation [25–35]. Like protein vaccines, mRNA vaccines also rely on innate immune stimulation. Unlike protein vaccines, however, mRNA vaccines do not require traditional adjuvants but rely on mRNA delivery to antigen presenting cells (APCs) for antigen expression.

Here we investigated multiple LNP biophysical properties that could affect mRNA vaccine delivery and subsequent immune responses. The optimal size for protein vaccine adjuvants is dependent on the adjuvant material, how the antigen and adjuvant associate, and the desired vaccine response (e.g., humoral, cellular) [27,36]. Thus, to specifically investigate the role of particle size in vaccine potency, all other aspects of the delivery system must be matched. Herein, we changed mRNA LNP size independent of lipid composition for our CMV vaccine and systematically investigated the optimal mRNA LNP size for generating humoral immune responses. Our multi-antigenic CMV vaccine encodes for the viral surface pentamer complex comprised of five subunits (gH, gL, UL128, UL130, UL131A) plus envelope glycoprotein gB [5]. We found that within the sizes tested, CMV mRNA LNP vaccine antibody titers were strongly size-dependent in mice. In contrast, such LNP size effects were not observed in non-human primates (NHPs).

2. Methods

2.1. mRNA and lipid nanoparticle production

All cytomegalovirus (CMV) mRNA constructs used in this study were manufactured in vitro by T7 RNA polymerase-mediated transcription with complete replacement of uridine by N1-methyl-pseudouridine as previously described [37]. Briefly, the DNA template used in the in vitro reaction contained the immunogen open-reading frame flanked by 5' UTR and 3' UTR sequences and was terminated by a polyA tail. After transcription, the pre-mRNA was purified by oligo-dT affinity and the cap 1 structure was added to the 5′ end using Vaccinia capping enzyme (New England Biolabs, Ipswitch, MA) and Vaccinia 2′*O*-methyltransferase (New England Biolabs, Ipswitch, MA). The capped mRNA was then purified by reverse phase purification, buffer exchanged by tangential flow filtration into sodium citrate, pH 6.5, sterile filtered, and kept frozen at −20 °C until further use.

LNPs were manufactured via nanoprecipitation by mixing the ionizable lipid H [12], distearoylphosphatidylcholine (DSPC), cholesterol, and PEG2k-DMG lipid dissolved in ethanol with all six CMV constructs pooled and diluted in sodium acetate buffer (pH 5.0) [5]. To obtain particles in a range of sizes, the aqueous and organic streams were mixed in volumetric flow ratios between 1:1 and 3:1 (aqueous: ethanol), and subsequently aged between 0 and 5 h prior to neutralization and buffer exchange. Formulations were concentrated as needed to obtain the final target concentration, passed through a 0.22 μm filter, and stored at 4 °C until use. An additional dilution step into 5% dextrose in water (D5W) was applied to select LNP formulations to further modulate particle size. All formulations were tested for particle size, mRNA encapsulation, and endotoxin levels and were deemed acceptable for in vivo study.

2.2. Dynamic light scattering (DLS)

Average LNP size was determined by dynamic light scattering (DLS) using the Wyatt DynaPro Plate Reader II (Santa Barbara, CA). Samples were diluted in PBS at volumetric ratios of 1:30–1:75 prior to testing.

2.3. Nanoparticle tracking analysis (NTA)

The Malvern Nanosight NS300 (Malvern Panalytical, Worcestershire, UK) was used for nanoparticle tracking analysis (NTA). Samples were diluted 5000–40,000 fold in 1× PBS pH 7.2 to a final concentration of 100–250 particles per frame. Four, thirty second videos were taken for analysis to generate population histograms. The mean, mode, SD, D10, D50, D90, and particle count of the merged data was determined using the NanoSight software. The population span was calculated as follows: (D90-D10)/D50.

2.4. Particle count by coulter counter

Formulations were analyzed for number of particles sized 800–10,000 nm in diameter using the Multisizer 4e Coulter Counter with a 30 μM aperture (Beckman Coulter, Indianapolis, IN). Samples were diluted 130–201 fold in 1× PBS pH 7.2 to achieve total particle counts in the range of 5000–20,000 particles. To account for concentration differences between formulations, particle counts were normalized to the total mRNA present in the formulation.

2.5. mRNA entrapment

mRNA encapsulation efficiency was determined by the Quant-iT Ribogreen RNA assay (Life Technologies, Burlington, ON) as previously described [38]. Briefly, LNP-mRNA formulations were incubated with the Ribogreen reagent in the presence and absence of 2% Triton X-100 (Sigma-Aldrich, St. Louis, MO). Fluorescence intensities (excitation/emission: 480/520 nm) were measured for total mRNA bound to Ribogreen dye after release from LNP by Triton X-100 and unencapsulated mRNA bound to Ribogreen dye in the absence of Triton X-100.

2.6. Cryogenic electron microscopy (Cryo-EM)

To prepare cryoEM grids, 2.5 μL of sample was applied to a Quantifoil 200 mesh grid (Quantifoil; Großlöbichau, Germany), manually blotted for ~3–4 s with filter paper, and then plunged into liquid ethane. The image was collected on a FEI Tecnai TF20 at an accelerating voltage of 200 kV using TVIPS EM-Menu program. The instrument is equipped with a 16-megapixel CCD camera. The nominal magnification used was 29,000 and 50,000 with 2 binning.

2.7. Characterization of LNP surface polarity

LNP surface polarity was characterized using a modified version of a method previously described for liposomes [39]. Briefly, a fluorophore, 6-dodecanoyl-*N*,*N*-dimethyl-2-napthylamine (Laurdan), was dissolved in dimethyl sulfoxide (DMSO) and then incubated with LNPs for 3 h at room temperature with lipid to Laurdan molar ratio at approximately 600 to 1 and DMSO to aqueous buffer volume ratio of 1 to 500. After excitation at 340 nm, the fluorescence spectrum of Laurdan with each LNP was recorded at emission wavelengths 400–600 nm using a FluoroMax spectrofluorometer (Horiba; Kyoto, Japan). The generalized polarization (GP) of Laurdan is calculated as follows: $GP = \frac{I_{435}-I_{490}}{I_{435}+I_{490}}$, where I_{435} and I_{490} are emission intensities at 435 and 490 nm, respectively. The normalized *GP* (*N-GP*) was then calculated using the following equation: $N\text{-}GP = \frac{GP-GP_{min}}{GP_{max}-GP_{min}}$, where GP_{max} is 0.6 and GP_{min} is 0.3.

2.8. Small-angle X-ray scattering (SAXS)

Small-angle X-ray scattering experiments were performed using a SAXSpoint 2.0, from Anton Paar following a similar protocol described elsewhere [40]. A Primux 100 micro-X-ray source was used to generate x-rays at wavelength of 0.154 nm. The scattered intensity was collected using a two- dimensional (2D) EIGER R series CMOS detector from

DECTRIS at a sample to detector distance of 575 mm. The 2D data was then circularly averaged, yielding the one-dimensional (1D) SAXS profile with wave vector q ranging from 0.06 nm^{-1} to 4 nm^{-1}, where q is expressed using the following equation, $q = \frac{4\pi}{\lambda} sin\left(\frac{\theta}{2}\right)$, with λ and θ being the wavelength and scattering angle, respectively. The 1D data was further corrected for sample transmittance and buffer background.

2.9. Immunogenicity in mice

Animals were immunized as previously described [5,41]. Briefly, we immunized six to eight-week old female BALB/c mice (Charles River Laboratories International, Inc.; Wilmington, MA) by intramuscular injection with 50 μL of the indicated mRNA LNP formulations on days 1 and 22. Each dose contained 3 μg of mRNA. Approximately 100 μL of blood was collected from mice via tail vein and centrifuged at 1200 xg for serum isolation (10 min at 4 °C). Serum was stored at −80 °C until analysis by ELISA. All mouse studies were approved by the Animal Care and Use Committee at Moderna and followed NIH and National Research Council guidelines for animal experiments and husbandry.

2.10. Immunogenicity in non-human primates (NHP)

NHP studies were conducted at Charles River Laboratories (Sherbrooke, QC, Canada) using naive cynomolgus monkeys, 2–5 years old and weighing 2–5 kg. Animals were housed in stainless steel, perforated-floor cages, in a temperature- and humidity-controlled environment (20–26 °C and 30–70%, respectively), with an automatic 12-h/12-h dark/light cycle. Animals were fed PMI Nutrition Certified Primate Chow No. 5048 twice daily. Tuberculin tests were carried out on arrival at the test facility. The study plan and procedures were approved by preclinical services Sherbrook (PCS-SHB) IACUC. Animal experiments and husbandry followed NIH (Publication no.8023, eighth edition), U.S. National Research Council, and Canadian Council on Animal Care (CCAC) guidelines.

To evaluate immunogenicity, cynomolgus monkeys received 30 μg mRNA encoding CMV pentamer and gB formulated in small (64 nm), medium (81 nm), large (108 nm), or extra-large (146 nm) LNPs on days 1 and 22. Injections were given intramuscularly in a volume of 0.5 mL. Blood was collected on day 0, 22, and 36 from a peripheral vein and centrifuged at 2400 xg for 10 min at 4 °C for separation of serum. If an immunization and blood collection occurred on the same day, the blood collection was done first. Serum was stored at −80 °C for later analysis.

2.11. Enzyme linked immunosorbent assay (ELISA)

Total immunoglobulin G (IgG) antibody titers against CMV pentamer or gB were measured by ELISA. Briefly, 96-well plates were coated with 2 μg/mL of CMV pentamer complex (Native Antigen Company) or 1 μg/mL gB (Sino Biological) protein overnight. Serial dilutions of serum were added and bound antibody detected with horseradish peroxidase (HRP)-conjugated goat anti-mouse IgG (Southern Biotech) or HRP-conjugated anti-NHP IgG (Southern Biotech) depending on species, followed by incubation with TMB substrate (KPL). The absorbance was measured at OD450 nm. Titers were determined using a four-parameter logistic curve fit in GraphPad Prism (GraphPad Software, Inc.) and defined as the reciprocal serum dilution at approximately OD450 nm = 0.4 (normalized to a standard on each plate).

2.12. Statistical modeling for the impact of LNP size on antibody titer

To model the impact of particle size on antibody titer we used B-splines. This approach provides the flexibility of assessing a specific "knot" at which point the trend of immunogenicity begins to change with respect to particle size. We searched for the best-fitted knot from 85 to 170 nm, at 5 nm increment, for antibody titer responses post the prime dose, and from 75 to 170 nm at 5 nm increment for antibody titers post the boost dose. We used cross-validation to compare and select the best-fitted knot with quadratic B-splines. Specifically, for each dataset (after each vaccination for both anti-pentamer and anti-gB titers), we split the animal samples into training data and testing data. The training data is used to estimate predicted B-splines at some chosen knot. The testing data is used to assess the fit of the predicted B-splines, and to compute the proportion of variance explained (PVE) for assessing predictive fit. The PVE is calculated as the sum of squared differences between the predicted titers and the mean titer divided by the sum of squared differences between the individual animal titers and the mean titer. Fig. S1 shows the PVE results of 3-fold, 4-fold and 5-fold cross-validation across 20 random seeds.

3. Results

3.1. Retrospective analysis

Given the potential for particle size to impact vaccine potency, we performed a retrospective analysis of 24 CMV vaccine immunogenicity studies evaluating 135 LNP lots previously tested in mice. Available biophysical data for all LNPs were average particle size (determined by dynamic light scattering; DLS) and RNA entrapment (determined by Quant-iT RiboGreen dye binding). In every study, the same immunization schedule had been followed: female BALB/C mice were injected twice intramuscularly, three weeks apart and then serum was collected three weeks after the first (prime) dose and two weeks after the second (boost) dose (Fig. 1A). Each dose contained a total of 3 μg mRNA encoding CMV pentamer and gB, which is in the dynamic range of the vaccine [5]. Immunogenicity was measured using an enzyme linked immunosorbent assays (ELISA) for antibodies against CMV pentamer and gB antigens to calculate antibody titer. To minimize any confounding influence of low mRNA entrapment on immunogenicity, we limited our analysis to only those LNPs which RNA entrapment was >85%.

Plotting mRNA entrapment versus average particle diameter (Fig. 1B) revealed no clear relationship between these two parameters, which was confirmed by Spearman's correlation ($r_{spearman} = -0.081$, $p = 0.41$). Similarly, there was no statistically significant trend between mRNA entrapment and CMV pentamer ($r_{spearman} = -0.046$, $p = 0.6396$) or gB immunogenicity ($r_{spearman} = 0.313$, $p < 0.01$) (Fig. 1C). In contrast, plotting antibody titer against particle size revealed a strong relationship after the second dose for both CMV pentamer ($r_{spearman} = 0.676$, $p < 0.001$) and gB ($r_{spearman} = 0.484$, $p < 0.001$) titers. Visual inspection of the data post boost suggested a hyperbolic relationship – immunogenicity was strongly dependent on particle size for particle size around or below 80–90 nm, but for particles above 80–90 nm antibody titers were consistently high (Fig. 1D). After the first dose, pentamer titers increased with increasing particle size. The trend was less clear with gB titers post prime, as many of the groups reported titers below the limit of detection.

After studying the impact of LNP size on CMV immunogenicity, we wondered if the trend would hold true for other mRNA vaccines containing only a single construct or secreted antigens. Historical data were mined for the impact of size on immunogenicity using influenza H10N8, chikungunya and zika virus vaccine constructs. These data sets were more limited than the CMV analysis, nonetheless all data were supportive of the findings described with the CMV vaccine (Fig. S2).

3.2. Changing LNP size with formulation process variables

Although the retrospective analysis suggested a strong relationship between particle size and vaccine immunogenicity, it covered a broad range of lipid compositions (various ionizable lipids, phospholipids, sterols, and PEG lipids), lipid molar ratios, and formulation processes. To isolate particle size as a single variable, we next sought ways to systematically vary particle size while keeping the lipid components and

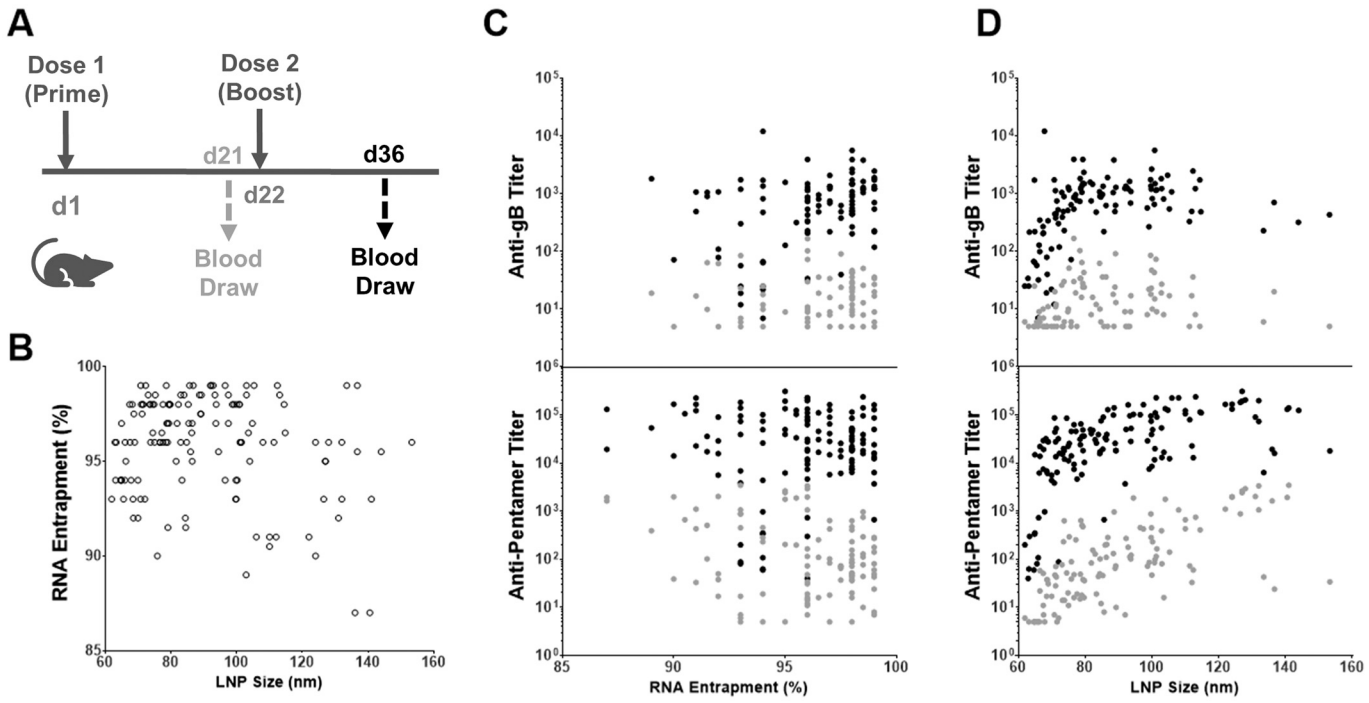

Fig. 1. CMV Murine Immunogenicity Retrospective Analysis A retrospective analysis of the relationship between LNP size, RNA entrapment, and antibody titer for 135 LNP formulations tested in 24 CMV vaccine immunogenicity studies ($n = 5$–10 mice/LNP). All studies followed the same immunization schedule (A) and used the same 3 μg mRNA dose level. RNA entrapment was plotted against LNP size (B), anti-gB titer (C, top) and anti-pentamer titer (C, bottom). LNP size was plotted against anti-gB titer (D, top) and anti-pentamer titer (D, bottom).

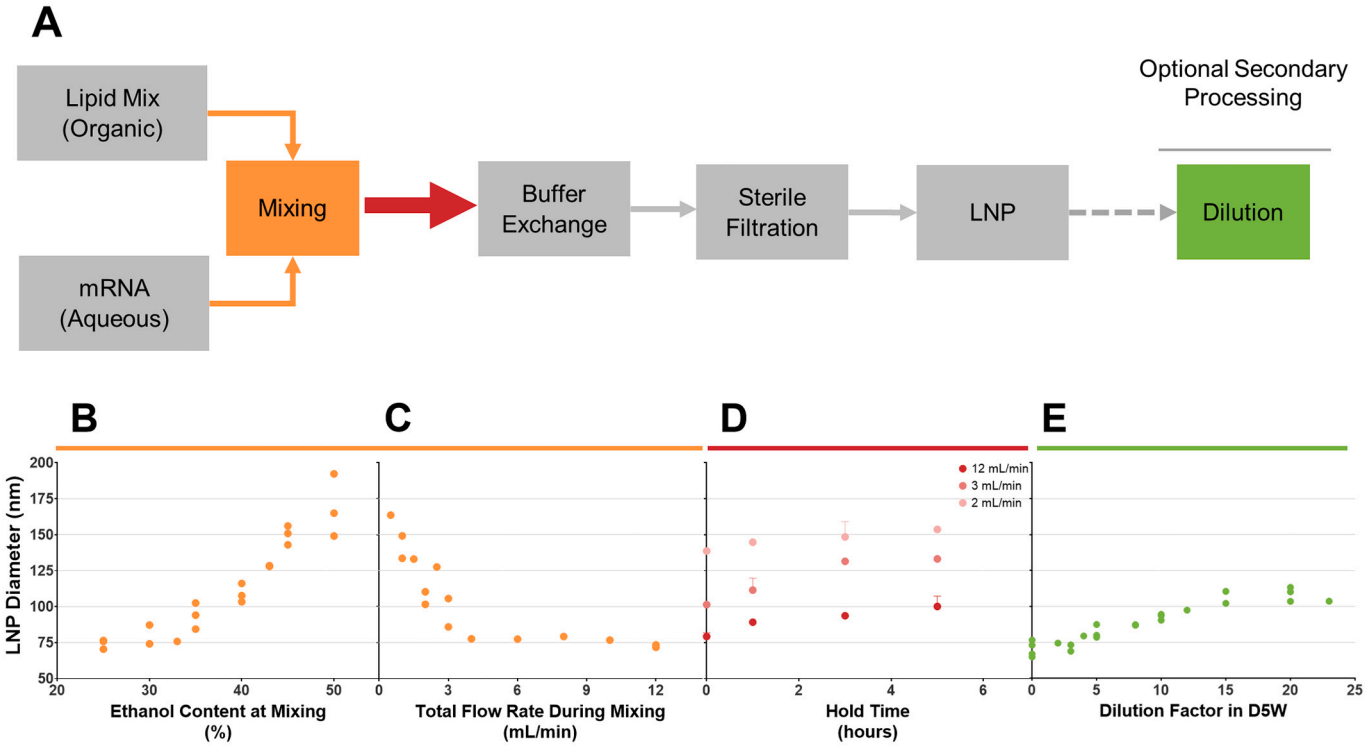

Fig. 2. Methods of Changing LNP Size LNP size was changed by modifying formulation process parameters. The formulation process was modified at the mixing event, the time prior to buffer exchange or through optional secondary processing steps once LNPs were prepared (A). Figs. B-E shown the average LNP size measured by DLS after varying the volumetric percentage of ethanol present at mixing while holding flow rate constant at 12 mL/min (B), the total flow rate during mixing while holding volumetric percentages constant at 25% ethanol (C), the time held between mixing and buffer exchange for multiple flow rates at a volumetric percentage of 30% ethanol (D), or LNP dilution in a 5% dextrose solution (E). Data is color coded according to the process step being varied as depicted in the process diagram (A).

composition constant. To assess this relationship, we used our previously published optimized vaccine ionizable lipid, lipid H [12]. To prepare LNPs (Fig. 2A), lipids are first dissolved in ethanol and then mixed with an acidified aqueous solution of mRNA to allow particle formation by nanoprecipitation. Once particles have formed, acetate-buffered ethanol is replaced with a physiologically relevant buffer by buffer exchange. The desired final LNP concentration is achieved by concentration and dilution prior to a final sterile filtration step. An optional secondary processing step of dilution after filtration can be applied if warranted.

Previous studies have demonstrated that LNP and liposome size can be modulated by changing the volumetric ratio of the ethanol and aqueous streams as well as total mixing flow rate [42–45]. When we applied these concepts to our LNP formulations, we observed that increasing ethanol from 25 to 50% during mixing (*v*/v) led to larger LNPs (Fig. 2B). In this study we did not test ethanol concentrations above 50% because in our experience this generally leads to low RNA entrapment and increased particle heterogeneity. Regarding flow rate, decreasing total flow through a small-scale mixing device from 12 to 0.5 mL/min while keeping the ethanol percentage constant (25%) also led to larger particles (Fig. 2C). Thus, our LNPs exhibited similar behavior to other lipid-based systems regarding ethanol percentage and flow rate at mixing.

We also experimented with varying other process steps, but many exhibited poor reproducibility and/or resulted in low RNA entrapment values. However, we were able to identify two additional process variables that yielded reliable and reproducible particle size changes. At 30% ethanol during mixing, implementing a hold time of up to 5 h prior to buffer exchange reliably increased LNP size (Fig. 2D). Additionally, following sterile filtration, particle size could be further manipulated by diluting the LNPs into a 5% dextrose solution (D5W) – as the dilution factor increased, particle size also increased (Fig. 2E). With these methods combined, we were thus able to create a wide range of LNP particle sizes (60–200 nm) without changing lipid composition.

Changing formulation parameters to modulate particle size could impact other biophysical properties. Therefore, we characterized several biophysical properties, including particle size (as measured by DLS and Nanoparticle Tracking Analysis, NTA), particle count by Coulter (800–10,000 nm), RNA entrapment, storage conditions (pH, osmolality) and surface polarity. DLS enabled us to determine the average particle size and polydispersity index (PDI), while NTA yielded the mean, mode, and span of the particle population. When we tested for correlations between all measured properties (Fig. 3), we found that all orthogonal size measurements strongly correlated with one another ($|r_{spearman}|$ range between 0.82 and 0.97). Conversely, the number of particles greater than 800 nm measured by Coulter did not correlate with size, demonstrating that we were modulating the main LNP population and not adding larger aggregates as LNP size increased. A negative correlation between average particle size and particle surface polarity was also observed ($r_{spearman} = -0.51$). As particle size increases, the total number of particles will decrease as well as the ratio of surface area to volume, leading to changes in surface polarity likely due to a greater number of amphipathic molecules (e.g., DSPC, PEG-lipid) on the LNP surface. Other biophysical measurements such as RNA encapsulation efficiency, pH, and osmolality did not correlate with LNP size measurements. Thus, by using multiple methods to modulate particle size we can isolate size as a variable allowing us to specifically investigate the relationship between LNP size and immunogenicity.

3.3. Relationship between LNP size and murine immunogenicity

To evaluate the impact of changing particle size without changing lipid composition, we tested the CMV pentamer and gB LNPs generated above (Fig. 2) for immunogenicity in mice, following the same immunization and blood draw schedule as in Fig. 1A. Plotting pentamer and gB titers after both the prime and boost doses versus particle size with

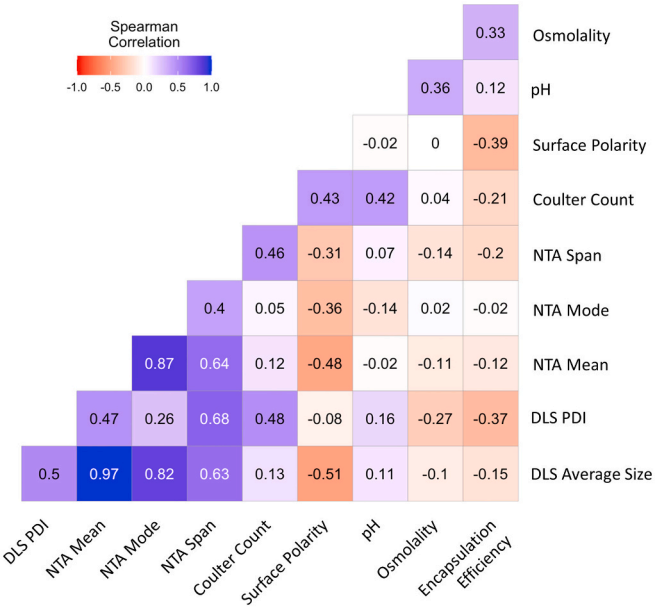

Fig. 3. Correlations Between Measured LNP Properties Spearman correlations between measured biophysical characteristics. Properties measured include average size and polydispersity index (PDI) measured by DLS, particle mean, mode, and span measured by Nanoparticle Tracking Analysis (NTA), particle count by Coulter Multisizer (800–10,000 nm), % RNA encapsulation efficiency measured by the RiboGreen assay, pH, osmolality, and surface polarity as measured by Laurdan dye.

these more controlled formulations (Fig. 4) validated the observations from the retrospective analysis (Fig. 1). Although we observed a moderate correlation between LNP size and surface polarity (Fig. 3), plotting pentamer and gB titers versus surface polarity yielded no visible trends (Fig. S3).

The immunogenicity results indicate that after the prime dose, anti-pentamer titers increased with particle size up to 105 nm and then decreased at larger sizes (Fig. 4A). After the boost, this positive relationship between size and immunogenicity was even stronger for LNP formulations less than 85 nm, while all LNPs above 85 nm yielded similar anti-pentamer titers (Fig. 4B). These inflection points were based on statistical modeling of the data, excluding samples with titers below the lower limit of quantification (LLOQ). When sera were analyzed for CMV pentamer titers three weeks after the prime dose, 52 of 192 serum samples were below LLOQ, whereas only 2 of 192 serum samples collected two weeks after the boost were below LLOQ, both being in the group immunized with smallest LNPs (67 nm).

Anti-gB titers yielded similar but less striking results (Fig. 4C–D). When sera were analyzed for CMV gB titers three weeks after the prime dose, 72 of 192 samples were below LLOQ. Inflection point modeling of the 120 samples above the LLOQ revealed no effect of LNP size on gB immunogenicity (Fig. 4C). After the boost dose, however, all anti-gB titer levels were above the LLOQ. Infection point modeling of these 192 samples revealed that anti-gB titer increases with particle size up to 110 nm and then plateaued at larger sizes (Fig. 4D).

3.4. Advanced characterization of LNPs used in parallel mouse and NHP immunogenicity studies

Having observed a strong dependence of immunogenicity on particle size in mice, we next wanted to assess the impact of this biophysical property in primates. To do so, we generated four formulations with different particle sizes (categories with average sizes: small, 64 nm; medium, 81 nm; large, 108 nm; extra-large, 146 nm; Fig. 5) using the previously characterized process variables. In the size ranges readily

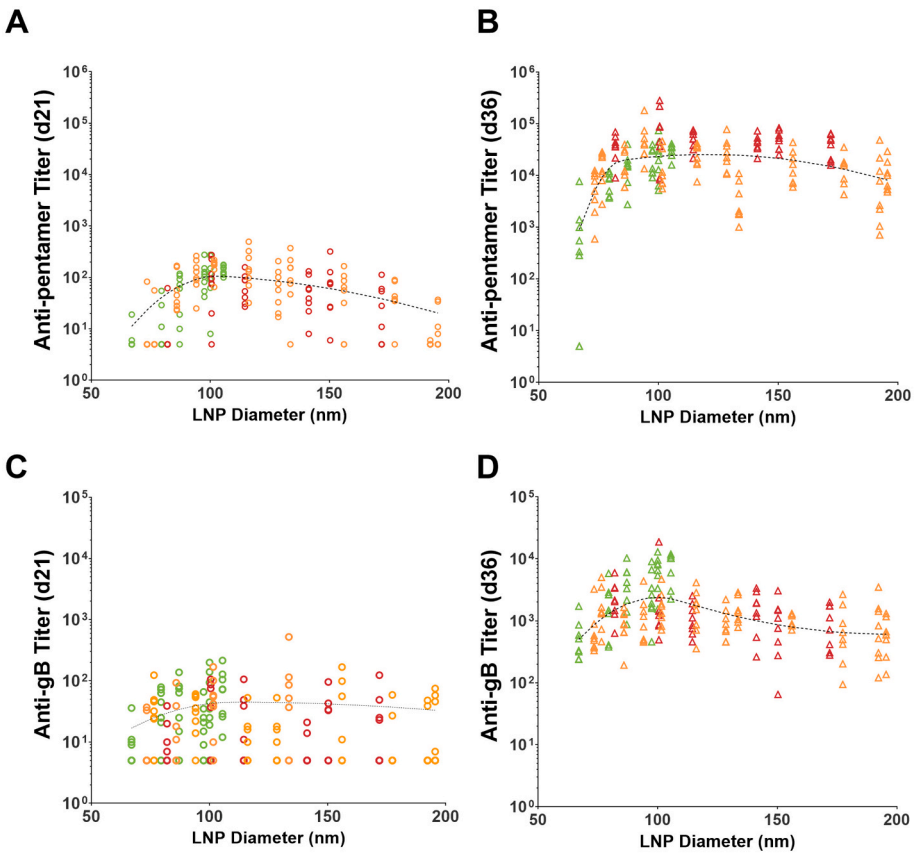

Fig. 4. LNP Size and Murine Immunogenicity Mice received prime and boost immunizations of different sized LNPs encapsulating mRNA encoding CMV pentamer and gB antigens at days 1 and 22; each dose contained 3 μg mRNA. Anti-CMV pentamer and anti-gB IgG antibody titers were measured three weeks after the prime (A, C) or two weeks after the boost (B, D). Data points show the antibody titers for individual animals (n = 8/group). The dotted lines depict the modeled impact of particle size on immunogenicity based on statistical analysis of the individual animal titers after each immunization. The color scheme corresponds to the process parameter being modified to change LNP size as defined in Fig. 2A.

detectable by DLS (0.5–1000 nm), all four formulation conditions generated monodisperse populations (PDI < 0.14) (Fig. 5A). Throughout in vivo dosing, the particle size remained constant when measured by DLS, indicating particle stability through 4 °C storage over several weeks.

To minimize size biases due to light scattering, we also measured particle size and distribution by NTA (Fig. 5B). In addition to confirming a gradual shift from smaller to larger particles across the four formulations, NTA revealed an inverse correlation between particle size and particle count. This was expected because identical mRNA and lipid input amounts were used for each formulation – as particle size increases there should be fewer particles for a given input amount of mRNA, with large particles containing more mRNA molecules than smaller particles. NTA also revealed a broadening of the size distribution as average particle size increased. Coulter counting revealed that all formulations contained a similar number of particles greater than 800 nm ($\sim 10^6$ per mg mRNA). We estimate that <0.0001% of particles are greater than 800 nm given that NTA calculated $\sim 10^{12}$ particles per mg mRNA in the range of 1 to 700 nm. Therefore, no formulation contained a significant population of large aggregates.

As a visual confirmation of these findings, cryogenic electron microscopy (cryo-EM) images showed a particle size increase from small to extra-large formulations, with a shift in individual particle size as well as a greater range of particle sizes per image with the larger particle formulations (Fig. 5C). Moreover, for small particles, cryo-EM images showed electron dense regions, whereas organized lamellar structure was observed on the surface of larger particles. Consistent with the imaging results, SAXS profiles showed more pronounced lamellar structure only in larger sized particles as reflected from the sharper peak at $q \sim 1\ nm^{-1}$ (Fig. 5D), which is characteristic of an organized lamellar phase resulting from the mRNA association with the bilayer [40,46,47]. In addition, the LNP surface was found to be less polar with increasing particle size (Fig. 5E). These results demonstrate that changes in LNP size also leads to changes in the mRNA organization and LNP surface properties.

3.5. Relationship between LNP size and murine/NHP immunogenicity

In murine and NHP immunogenicity studies for this set of LNPs, we measured antibody titers against both the CMV pentamer and gB components of the vaccine. Consistent with previous data, the medium, large, and extra-large LNPs produced higher pentamer antibody titers in mice than the small LNPs ($p < 0.001$, Tukey's Test) after the boost (Fig. 6A-B). In NHPs, all LNPs tested produced robust immune responses against the CMV pentamer and no one size population produced a statistically different antibody response (Tukey's Test, $p > 0.05$) (Fig. 6C). Although, all sizes produced higher anti-gB titers than the pre-study value, the responses were not statistically different since the cynomolgus monkeys were seropositive for gB at the start of the study (Fig. 6D).

4. Discussion

Of all the biophysical properties we examined here, LNP size showed the strongest correlation with murine mRNA vaccine immunogenicity as measured by total antibody titer. An efficacious mRNA vaccine requires protein antigen expression followed by an antigen-specific immune response. Once injected intramuscularly, APCs including neutrophils, monocytes, macrophages, and dendritic cells (DCs) take up LNPs at both the injection site and in draining lymph nodes [48]. LNP uptake results in a local, transient type I interferon (IFN) response [48–50] and protein expression in monocytes and myeloid DCs [43] [48–50]. This innate immune activation combined with antigen expression results in a potent antigen-specific immune response [51]. Literature suggests that non-LNP particles smaller than 200 nm freely drain to the lymph nodes, whereas those larger than 200 nm require local uptake and subsequent

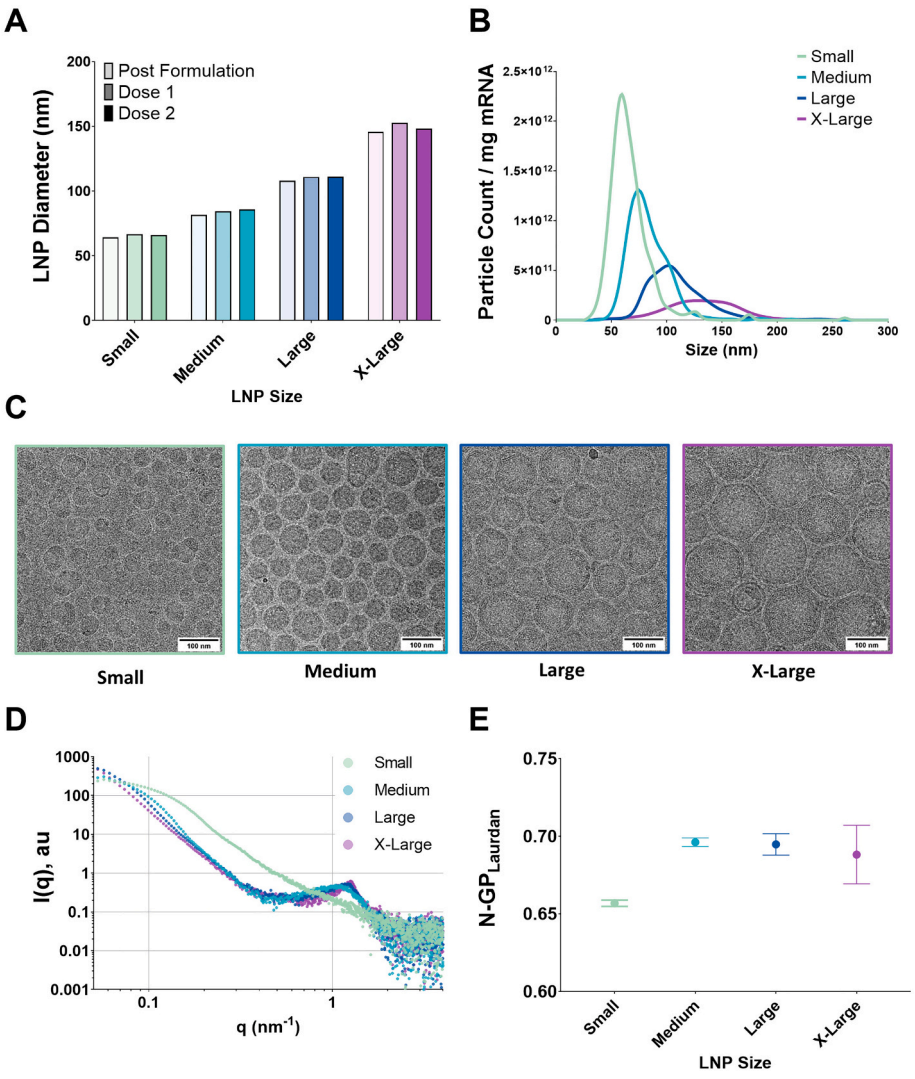

Fig. 5. Heightened Characterization of Select Formulations Advanced size, structure and surface characterization of select LNPs used in the NHP evaluation. Average particle diameter by DLS (A), particle size distribution by NTA (B), cryo-EM images (C), LNP structure by SAXS analysis (D), generalized polarization by Laurdan for probing LNP surface (E). Error bars represent the standard deviation of technical replicates ($n = 3$).

transport by APCs [51–55]. Particle size can also influence vaccine-APC interactions and particle localization in lymph node structures (e.g., subcapsular sinus) [24,53]. For mRNA vaccines, LNP uptake by APCs is necessary for generating antigen-specific immunity [15]. Particles between 500 and 5000 nm are preferentially taken up by macrophages, whereas particles 20–200 nm are preferentially taken up by DCs [56]. We have previously shown that mRNA vaccine LNPs sized 80–100 nm elicit APC uptake and antigen expression [48]. In this study, we evaluated the effects of a broader particle size range on immunogenicity.

Using a fixed lipid composition and controlled process parameters, we formulated various LNP particle sizes ranging from 60 to 200 nm. Previous reports have described LNP size control for DNA and small interfering RNA (siRNA) delivery by modulating either total flow rate or flow rate ratio during mixing [42,44]. Consistent with those reports, we were able to decrease particle size of mRNA LNPs by increasing the total volumetric flow rate during mixing [42,44,45] and increasing the aqueous-to-ethanol stream ratio [43,45]. Modifying such mixing parameters changes the dynamics of the nanoprecipitation reaction and solubility of the lipid components [42,44,45]. Increasing the total volumetric flow rate during formulation increases mixing efficiency and decreases the time scale of particle formation, resulting in smaller particles [44]. Conversely, decreasing the aqueous-to-ethanol stream ratio increases ethanol concentration at the mixing interface, thus increasing lipid solubility and lengthening particle formation time, allowing for more particle growth [45]. We found that introducing a hold time between the mixing event and buffer exchange further increased particle size, an additional method not previously described in the literature. We hypothesize the hold time enables more uniform ethanol diffusion prior to buffer exchange, thus increasing the timescale of particle assembly and particle size growth [45]. Additionally, diluting buffer-exchanged LNPs into a dextrose solution also increased LNP particle size. Other reports in the literature have changed particle size by varying the molar percent of the PEG lipid [38,57,58]; we did not employ this method as we wanted to eliminate lipid composition as a variable.

Limited knowledge exists for how modulating the particle size of lipid-based systems without changing lipid composition impacts local delivery. Literature on subcutaneous administration shows smaller lipid particles leave the injection site more readily than larger particles, allowing them to drain more efficiently to lymph nodes [58–60]. However, particles too small may not be efficacious even if they are able to escape the local subcutaneous injection site [58], demonstrating the need for an optimum size to enable both efficient lymph node drainage and cellular interactions. To our knowledge, no published work modulating particle size of lipid-based systems has evaluated efficacy after

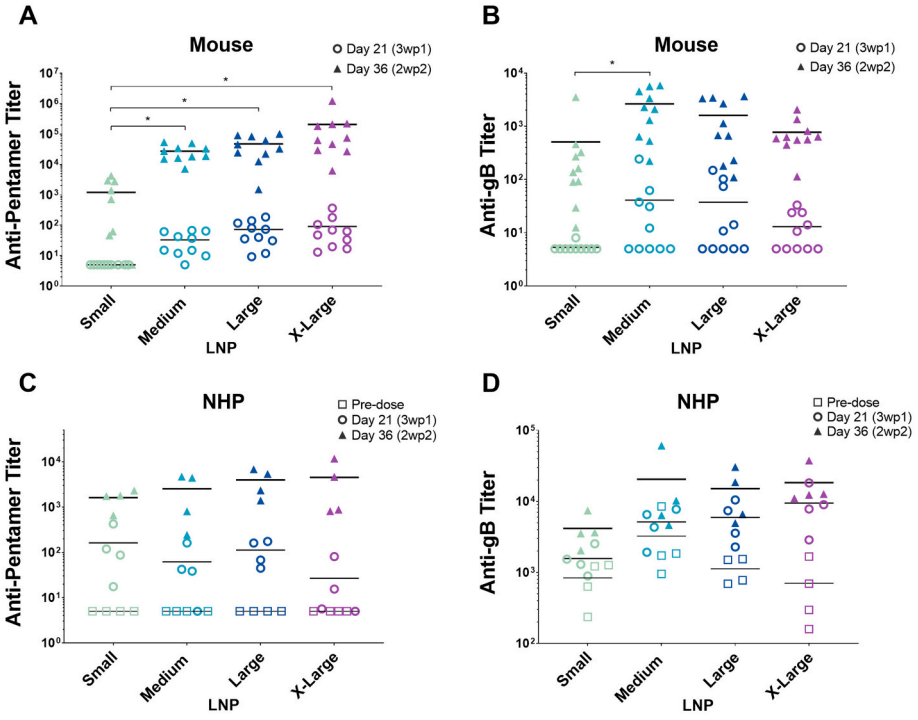

Fig. 6. LNP Size and Primate Immunogenicity Mice and NHP were immunized with small (64 nm), medium (81 nm), large (108 nm) and extra-large (146 nm) LNPs containing mRNA encoding CMV pentamer and gB. Anti-pentamer IgG titers (A, C) and anti-gB IgG tiers (B, D) were measured in mice and NHP prior to dosing, three weeks after the prime and two weeks after the boost. (Statistical significance measured by Tukey's Test; * $p < 0.001$).

intramuscular delivery.

Unlike protein vaccines that require a particulate adjuvant to stimulate an innate immune response, mRNA vaccines are not adjuvanted. Instead, mRNA vaccine LNPs facilitate drainage to lymphoid tissues, cellular uptake, and in situ antigen expression, thus mimicking a viral infection to generate an immune response. Yet the literature investigating the role of particle size in vaccine potency is largely focused on protein antigens formulated with particulate adjuvants. In contrast to findings in that field, indicating smaller particles were more immunogenic [32,34,61], we found that smaller size mRNA LNPs were not more potent for inducing immune responses. One reason for this difference may be the range of sizes tested. Adjuvant literature often compares microparticles to nanoparticles [32,61], whereas our studies focused on a narrower range of particle size (60–200 nm). We also differ from vaccine adjuvants in the type of materials our particles are made of and the multiple roles that our nanoparticles play for successful delivery of mRNA (e.g., biodistribution, cell uptake and endosomal escape).

When looking to nature, viruses can vary dramatically in size and morphology, from as small as 12 nm to upwards of 750 nm [62,63]. Our optimally sized mRNA vaccine LNPs (~100 nm) are comparably sized to viruses such as SARs-COV-2 (100 nm), influenza A (80–120 nm), and mature HIV particles (100 nm) [64–66]. We hypothesize the optimal mRNA vaccine size facilitates immune cell recruitment to the injection site [26]. Particle size has been shown to impact cell recruitment of nanoparticles; 160 nm emulsion droplets recruit a greater number of immune cells to the injection site when compared to smaller particles of identical composition (20 and 90 nm) [26]. Additionally, the 160 nm particles resulted in the highest number of antigen-positive immune cells within the draining lymph node. Similarly, we would expect optimal mRNA vaccine LNPs are large enough to enhance immune cell recruitment yet small enough to facilitate APC uptake and subsequent antigen expression, driving a more robust antibody response. Cellular uptake can occur through pinocytosis, phagocytosis or be receptor mediated [67–69]. All mRNA LNPs tested are below the minimum particle size considered favorable for phagocytosis (500 nm) [70,71]. Spherical viruses similarly sized to our LNPs such as influenza (80 nm) and reovirus (120 nm) are taken up through receptor mediated endocytosis [68,72,73], however kinetics of entry may differ depending on particle size [71,72,74]. Similarly, we expect that we are not changing the mechanism of mRNA LNP uptake within the size range we tested but may be changing the kinetics of LNP entry into the cell.

In mice, we found that after the priming dose, antibody titer increased with increasing LNP size until ~100 nm, where antibody titer started to decrease. After a second dose, we observed antibody titers increasing with size for LNPs smaller than 85 nm and consistently high responses for particles larger than 85 nm. In NHPs, all particle sizes tested produced a robust immune response, with no impact of LNP size on immunogenicity over the size range tested (60–150 nm). To our knowledge, the role of vaccine particle size on immunogenicity has not previously been reported in primates. We speculate that our observed differences between mouse and NHPs may be due to anatomical differences between lymphatic vessels – it is possible that the smaller scale murine lymphatics are more sensitive to particle size within the range we tested than are the larger primate lymphatics. Hence, optimal mRNA vaccine particle size determined in rodents may not translate to primates.

Understanding the impact of LNP biophysical parameters on immunogenicity represents an important step for enabling rapid development of potent mRNA vaccines against new emergent diseases. Once an optimized delivery technology has been established, it can be used for all current and future mRNA vaccines. This platform approach allows for quick creation of a new vaccines once the antigen sequence is known [13,14]. Having shown that the effects of LNP size hold true across multiple different mRNA vaccines, we here demonstrate the platform nature of our mRNA vaccine delivery vehicles.

5. Conclusion

In this work, we developed a series of processes that allowed us to control mRNA LNP particle size independent of lipid composition. We

found that while mice require an average particles size around 100 nm for generating consistently high antibody titers, all particle sizes tested (60–150 nm) produced robust immune responses in non-human primates.

Acknowledgements

We acknowledge Jack Kramarczyk, Beth Lally, Mike Smith, Joe Schariter, Jaclyn Milton, Stephanie Kirby for brainstorming ways to change particle size, In Vivo Pharmacology at Moderna Inc. for conducting all mouse immunogenicity studies and Wong-Hoi Hui at the UCLA Cryo-EM facility for LNP images. This work was funded entirely by Moderna, Inc.

Appendix A. Supplementary data

Supplementary data to this article can be found online at https://doi.org/10.1016/j.jconrel.2021.05.021.

References

[1] R. Rappuoli, C.W. Mandl, S. Black, E.D. Gregorio, Vaccines for the twenty-first century society, Nat. Rev. Immunol. 11 (2011) 865–872, https://doi.org/10.1038/nri3085.
[2] V. Vetter, G. Denizer, L.R. Friedland, J. Krishnan, M. Shapiro, Understanding modern-day vaccines: what you need to know, Ann. Med. 50 (2017) 110–120, https://doi.org/10.1080/07853890.2017.1407035.
[3] A.S. Espeseth, P.J. Cejas, M.P. Citron, D. Wang, D.J. DiStefano, C. Callahan, G. O. Donnell, J.D. Galli, R. Swoyer, S. Touch, Z. Wen, J. Antonello, L. Zhang, J. A. Flynn, K.S. Cox, D.C. Freed, K.A. Vora, K. Bahl, A.H. Latham, J.S. Smith, M. E. Gindy, G. Ciaramella, D. Hazuda, C.A. Shaw, A.J. Bett, Modified mRNA/lipid nanoparticle-based vaccines expressing respiratory syncytial virus F protein variants are immunogenic and protective in rodent models of RSV infection, Npj Vaccines 5 (2020) 16, https://doi.org/10.1038/s41541-020-0163-z.
[4] P.R. Krause, S.R. Bialek, S.B. Boppana, P.D. Griffiths, C.A. Laughlin, P. Ljungman, E.S. Mocarski, R.F. Pass, J.S. Read, M.R. Schleiss, S.A. Plotkin, Priorities for CMV vaccine development, Vaccine. 32 (2013) 4–10, https://doi.org/10.1016/j.vaccine.2013.09.042.
[5] S. John, O. Yuzhakov, A. Woods, J. Deterling, K. Hassett, C.A. Shaw, G. Ciaramella, Multi-antigenic human cytomegalovirus mRNA vaccines that elicit potent humoral and cell-mediated immunity, Vaccine (2018), https://doi.org/10.1016/j.vaccine.2018.01.029.
[6] B. McCloskey, O. Dar, A. Zumla, D.L. Heymann, Emerging infectious diseases and pandemic potential: status quo and reducing risk of global spread, Lancet Infect. Dis. 14 (2014) 1001–1010, https://doi.org/10.1016/s1473-3099(14)70846-1.
[7] K.E. Jones, N.G. Patel, M.A. Levy, A. Storeygard, D. Balk, J.L. Gittleman, P. Daszak, Global trends in emerging infectious diseases, Nature. 451 (2008) 990–993, https://doi.org/10.1038/nature06536.
[8] S. Cleaveland, D.T. Haydon, L. Taylor, Wildlife and emerging zoonotic diseases: the biology, Circumst. Conseq. Cross-Spec. Transm. (2007) 85–111, https://doi.org/10.1007/978-3-540-70962-6_5.
[9] J.A. Lewnard, A.L. Reingold, Emerging challenges and opportunities in infectious disease epidemiology, Am. J. Epidemiol. 188 (2019) 873–882, https://doi.org/10.1093/aje/kwy264.
[10] K.G. Andersen, A. Rambaut, W.I. Lipkin, E.C. Holmes, R.F. Garry, The proximal origin of SARS-CoV-2, Nat. Med. 26 (2020) 450–452, https://doi.org/10.1038/s41591-020-0820-9.
[11] U. Sahin, K. Karikó, Ö. Türeci, mRNA-based therapeutics — developing a new class of drugs, Nat. Rev. Drug Discov. 13 (2014) 759–780, https://doi.org/10.1038/nrd4278.
[12] K.J. Hassett, K.E. Benenato, E. Jacquinet, A. Lee, A. Woods, O. Yuzhakov, S. Himansu, J. Deterling, B.M. Geilich, T. Ketova, C. Mihai, A. Lynn, I. McFadyen, M. Moore, J. Senn, M.G. Stanton, Ö. Almarsson, G. Ciaramella, L.A. Brito, Optimization of lipid nanoparticles for intramuscular administration of mRNA vaccines, Mol. Ther. Nucleic Acids. 15 (2019) 1–11, https://doi.org/10.1016/j.omtn.2019.01.013.
[13] L.A. Jackson, E.J. Anderson, N.G. Rouphael, P.C. Roberts, M. Makhene, R.N. Coler, M.P. McCullough, J.D. Chappell, M.R. Denison, L.J. Stevens, A.J. Pruijssers, A. McDermott, B. Flach, N.A. Doria-Rose, K.S. Corbett, K.M. Morabito, S. O'Dell, S. D. Schmidt, P.A.S. II, M. Padilla, J.R. Mascola, K.M. Neuzil, H. Bennett, W. Sun, E. Peters, M. Makowski, J. Albert, K. Cross, W. Buchanan, R. Pikaart-Tautges, J. E. Ledgerwood, B.S. Graham, J.H. Beigel, An mRNA Vaccine against SARS-CoV-2 — preliminary report, New Engl. J. Med. (2020), https://doi.org/10.1056/nejmoa2022483.
[14] K.S. Corbett, D.K. Edwards, S.R. Leist, O.M. Abiona, S. Boyoglu-Barnum, R. A. Gillespie, S. Himansu, A. Schäfer, C.T. Ziwawo, A.T. DiPiazza, K.H. Dinnon, S. M. Elbashir, C.A. Shaw, A. Woods, E.J. Fritch, D.R. Martinez, K.W. Bock, M. Minai, B.M. Nagata, G.B. Hutchinson, K. Wu, C. Henry, K. Bahi, D. Garcia-Dominguez, L. Ma, I. Renzi, W.-P. Kong, S.D. Schmidt, L. Wang, Y. Zhang, E. Phung, L.A. Chang, R.J. Loomis, N.E. Altaras, E. Narayanan, M. Metkar, V. Presnyak, C. Liu, M. K. Louder, W. Shi, K. Leung, E.S. Yang, A. West, K.L. Gully, L.J. Stevens, N. Wang, D. Wrapp, N.A. Doria-Rose, G. Stewart-Jones, H. Bennett, G.S. Alvarado, M. C. Nason, T.J. Ruckwardt, J.S. McLellan, M.R. Denison, J.D. Chappell, I.N. Moore, K.M. Morabito, J.R. Mascola, R.S. Baric, A. Carfi, B.S. Graham, SARS-CoV-2 mRNA vaccine design enabled by prototype pathogen preparedness, Nature (2020) 1–8, https://doi.org/10.1038/s41586-020-2622-0.
[15] K.A. Hajj, K.A. Whitehead, Tools for translation: non-viral materials for therapeutic mRNA delivery, Nat. Rev. Mater. 2 (2017) 17056, https://doi.org/10.1038/natrevmats.2017.56.
[16] S. Sabnis, E.S. Kumarasinghe, T. Salerno, C. Mihai, T. Ketova, J.J. Senn, A. Lynn, A. Bulychev, I. McFadyen, J. Chan, Ö. Almarsson, M.G. Stanton, K.E. Benenato, A novel amino lipid series for mRNA delivery: improved endosomal escape and sustained pharmacology and safety in non-human primates, Mol. Ther. (2018), https://doi.org/10.1016/j.ymthe.2018.03.010.
[17] S.L. Hewitt, A. Bai, D. Bailey, K. Ichikawa, J. Zielinski, R. Karp, A. Apte, K. Arnold, S.J. Zacharek, M.S. Iliou, K. Bhatt, M. Garnaas, F. Musenge, A. Davis, N. Khatwani, S.V. Su, G. MacLean, S.J. Farlow, K. Burke, J.P. Frederick, Durable anticancer immunity from intratumoral administration of IL-23, IL-36γ, and OX40L mRNAs, Sci. Transl. Med. 11 (2019), eaat9143, https://doi.org/10.1126/scitranslmed.aat9143.
[18] D. An, A. Frassetto, E. Jacquinet, M. Eybye, J. Milano, C. DeAntonis, V. Nguyen, R. Laureano, J. Milton, S. Sabnis, C.M. Lukacs, L.T. Guey, Long-term efficacy and safety of mRNA therapy in two murine models of methylmalonic acidemia, Ebiomedicine. 45 (2019) 519–528, https://doi.org/10.1016/j.ebiom.2019.07.003.
[19] N. Kose, J.M. Fox, G. Sapparapu, R. Bombardi, R.N. Tennekoon, A.D. de Silva, S. M. Elbashir, M.A. Theisen, E. Humphris-Narayanan, G. Ciaramella, S. Himansu, M. S. Diamond, J.E. Crowe, A lipid-encapsulated mRNA encoding a potently neutralizing human monoclonal antibody protects against chikungunya infection, Sci Immunol. 4 (2019), eaaw6647, https://doi.org/10.1126/sciimmunol.aaw6647.
[20] J.M. Richner, S. Himansu, K.A. Dowd, S.L. Butler, V. Salazar, J.M. Fox, J. G. Julander, W.W. Tang, S. Shresta, T.C. Pierson, G. Ciaramella, M.S. Diamond, Modified mRNA vaccines protect against zika virus infection, Cell 168 (2017) 1114–1125, e10, https://doi.org/10.1016/j.cell.2017.02.017.
[21] T. Schlake, A. Thess, M. Fotin-Mleczek, K.-J. Kallen, Developing mRNA-vaccine technologies, RNA Biol. 9 (2012) 1319–1330, https://doi.org/10.4161/rna.22269.
[22] K.J. Kauffman, J.R. Dorkin, J.H. Yang, M.W. Heartlein, F. DeRosa, F.F. Mir, O. S. Fenton, D.G. Anderson, Optimization of lipid nanoparticle formulations for mRNA delivery in vivo with fractional factorial and definitive screening designs, Nano Lett. 15 (2015) 7300–7306, https://doi.org/10.1021/acs.nanolett.5b02497.
[23] M. Jayaraman, S.M. Ansell, B.L. Mui, Y.K. Tam, J. Chen, X. Du, D. Butler, L. Eltepu, S. Matsuda, J.K. Narayanannair, K.G. Rajeev, I.M. Hafez, A. Akinc, M.A. Maier, M. A. Tracy, P.R. Cullis, T.D. Madden, M. Manoharan, M.J. Hope, Maximizing the potency of siRNA lipid nanoparticles for hepatic gene silencing in vivo, Angew. Chem. Int. Ed. 51 (2012) 8529–8533, https://doi.org/10.1002/anie.201203263.
[24] G.P. Howard, G. Verma, X. Ke, W.M. Thayer, T. Hamerly, V.K. Baxter, J.E. Lee, R. R. Dinglasan, H.-Q. Mao, Critical size limit of biodegradable nanoparticles for enhanced lymph node trafficking and paracortex penetration, Nano Res. 12 (2019) 837–844, https://doi.org/10.1007/s12274-019-2301-3.
[25] C. Foged, B. Brodin, S. Frokjaer, A. Sundblad, Particle size and surface charge affect particle uptake by human dendritic cells in an in vitro model, Int. J. Pharm. 298 (2005) 315–322, https://doi.org/10.1016/j.ijpharm.2005.03.035.
[26] R.R. Shah, M. Taccone, E. Monaci, L.A. Brito, A. Bonci, D.T. O'Hagan, M.M. Amiji, A. Seubert, The droplet size of emulsion adjuvants has significant impact on their potency, due to differences in immune cell-recruitment and -activation, Sci Rep-Uk. 9 (2019) 11520, https://doi.org/10.1038/s41598-019-47885-z.
[27] S. Yan, W. Gu, Z.P. Xu, Re-considering how particle size and other properties of antigen–adjuvant complexes impact on the immune responses, J. Colloid Interface Sci. 395 (2013) 1–10, https://doi.org/10.1016/j.jcis.2012.11.061.
[28] B. Slütter, W. Jiskoot, Sizing the optimal dimensions of a vaccine delivery system: a particulate matter, Expert Opin. Drug Del. 13 (2015) 167–170, https://doi.org/10.1517/17425247.2016.1121989.
[29] T. Fifis, A. Gamvrellis, B. Crimeen-Irwin, G.A. Pietersz, J. Li, P.L. Mottram, I.F. C. McKenzie, M. Plebanski, Size-dependent immunogenicity: therapeutic and protective properties of Nano-vaccines against tumors, J. Immunol. 173 (2004) 3148–3154, https://doi.org/10.4049/jimmunol.173.5.3148.
[30] I. Gutierro, R.M. Hernández, M. Igartua, A.R. Gascón, J.L. Pedraz, Size dependent immune response after subcutaneous, oral and intranasal administration of BSA loaded nanospheres, Vaccine. 21 (2002) 67–77, https://doi.org/10.1016/s0264-410x(02)00435-8.
[31] V. Kanchan, A.K. Panda, Interactions of antigen-loaded polylactide particles with macrophages and their correlation with the immune response, Biomaterials. 28 (2007) 5344–5357, https://doi.org/10.1016/j.biomaterials.2007.08.015.
[32] X. Li, A.M. Aldayel, Z. Cui, Aluminum hydroxide nanoparticles show a stronger vaccine adjuvant activity than traditional aluminum hydroxide microparticles, J. Control. Release 173 (2014) 148–157, https://doi.org/10.1016/j.jconrel.2013.10.032.
[33] K. Niikura, T. Matsunaga, T. Suzuki, S. Kobayashi, H. Yamaguchi, Y. Orba, A. Kawaguchi, H. Hasegawa, K. Kajino, T. Ninomiya, K. Ijiro, H. Sawa, Gold nanoparticles as a vaccine platform: influence of size and shape on immunological Responsesin Vitroandin vivo, ACS Nano 7 (2013) 3926–3938, https://doi.org/10.1021/nn3057005.
[34] R.R. Shah, D.T. O'Hagan, M.M. Amiji, L.A. Brito, The impact of size on particulate vaccine adjuvants, Nanomedicine-UK. 9 (2014) 2671–2681, https://doi.org/10.2217/nnm.14.193.
[35] Y.K. Katare, T. Muthukumaran, A.K. Panda, Influence of particle size, antigen load, dose and additional adjuvant on the immune response from antigen loaded PLA

microparticles, Int. J. Pharm. 301 (2005) 149–160, https://doi.org/10.1016/j.ijpharm.2005.05.028.
[36] D.S. Watson, A.N. Endsley, L. Huang, Design considerations for liposomal vaccines: influence of formulation parameters on antibody and cell-mediated immune responses to liposome associated antigens, Vaccine. 30 (2012) 2256–2272, https://doi.org/10.1016/j.vaccine.2012.01.070.
[37] J. Nelson, E.W. Sorensen, S. Mintri, A.E. Rabideau, W. Zheng, G. Besin, N. Khatwani, S.V. Su, E.J. Miracco, W.J. Issa, S. Hoge, M.G. Stanton, J.L. Joyal, Impact of mRNA chemistry and manufacturing process on innate immune activation, Sci. Adv. 6 (2020), eaaz6893, https://doi.org/10.1126/sciadv.aaz6893.
[38] S. Chen, Y.Y.C. Tam, P.J.C. Lin, M.M.H. Sung, Y.K. Tam, P.R. Cullis, Influence of particle size on the in vivo potency of lipid nanoparticle formulations of siRNA, J. Control. Release 235 (2016) 236–244, https://doi.org/10.1016/j.jconrel.2016.05.059.
[39] T.T. Bui, K. Suga, H. Umakoshi, Roles of sterol derivatives in regulating the properties of phospholipid bilayer systems, Langmuir Acs J. Surf. Colloids. 32 (2016) 6176–6184, https://doi.org/10.1021/acs.langmuir.5b04343.
[40] S. Patel, N. Ashwanikumar, E. Robinson, Y. Xia, C. Mihai, J.P. Griffith, S. Hou, A. A. Esposito, T. Ketova, K. Welsher, J.L. Joyal, Ö. Almarsson, G. Sahay, Naturally-occurring cholesterol analogues in lipid nanoparticles induce polymorphic shape and enhance intracellular delivery of mRNA, Nat. Commun. 11 (2020) 983, https://doi.org/10.1038/s41467-020-14527-2.
[41] K. Bahl, J.J. Senn, O. Yuzhakov, A. Bulychev, L.A. Brito, K.J. Hassett, M.E. Laska, M. Smith, Ö. Almarsson, J. Thompson, A. Mick Ribeiro, M. Watson, T. Zaks, G. Ciaramella, Preclinical and Clinical Demonstration of Immunogenicity by mRNA Vaccines against H10N8 and H7N9 Influenza Viruses, Mol. Ther. 25 (2017) 1316–1327, https://doi.org/10.1016/j.ymthe.2017.03.035.
[42] N. Kimura, M. Maeki, Y. Sato, Y. Note, A. Ishida, H. Tani, H. Harashima, M. Tokeshi, Development of the iLiNP device: fine tuning the lipid nanoparticle size within 10 nm for drug delivery, Acs Omega. 3 (2018) 5044–5051, https://doi.org/10.1021/acsomega.8b00341.
[43] M. Maeki, T. Saito, Y. Sato, T. Yasui, N. Kaji, A. Ishida, H. Tani, Y. Baba, H. Harashima, M. Tokeshi, A strategy for synthesis of lipid nanoparticles using microfluidic devices with a mixer structure, RSC Adv. 5 (2015) 46181–46185, https://doi.org/10.1039/c5ra04690d.
[44] Z. He, Y. Hu, T. Nie, H. Tang, J. Zhu, K. Chen, L. Liu, K.W. Leong, Y. Chen, H.-Q. Mao, Size-Controlled lipid nanoparticle production using turbulent mixing to enhance oral DNA delivery, Acta Biomater. 81 (2018) 195–207, https://doi.org/10.1016/j.actbio.2018.09.047.
[45] A. Jahn, W.N. Vreeland, D.L. DeVoe, L.E. Locascio, M. Gaitan, Microfluidic directed formation of liposomes of controlled size, Langmuir. 23 (2007) 6289–6293, https://doi.org/10.1021/la070051a.
[46] C.R. Safinya, I. Koltover, J. Raedler, DNA at membrane surfaces: An experimental overview, Curr. Opin. Colloid In. 3 (1998) 69–77, https://doi.org/10.1016/s1359-0294(98)80044-7.
[47] M.Y. Arteta, T. Kjellman, S. Bartesaghi, S. Wallin, X. Wu, A.J. Kvist, A. Dabkowska, N. Székely, A. Radulescu, J. Bergenholtz, L. Lindfors, Successful reprogramming of cellular protein production through mRNA delivered by functionalized lipid nanoparticles, Proc. National. Acad. Sci. 115 (2018) 201720542, https://doi.org/10.1073/pnas.1720542115.
[48] F. Liang, G. Lindgren, A. Lin, E.A. Thompson, S. Ols, J. Röhss, S. John, K. Hassett, O. Yuzhakov, K. Bahl, L.A. Brito, H. Salter, G. Ciaramella, K. Loré, Efficient targeting and activation of antigen-presenting cells in vivo after modified mRNA vaccine administration in rhesus macaques, Mol. Ther. 25 (2017), https://doi.org/10.1016/j.ymthe.2017.08.006.
[49] C. Pollard, J. Rejman, W.D. Haes, B. Verrier, E.V. Gulck, T. Naessens, S.D. Smedt, P. Bogaert, J. Grooten, G. Vanham, S.D. Koker, Type I IFN counteracts the induction of antigen-specific immune responses by lipid-based delivery of mRNA vaccines, Mol. Ther. 21 (2013) 251–259, https://doi.org/10.1038/mt.2012.202.
[50] A.D. Beuckelaer, C. Pollard, S.V. Lint, K. Roose, L.V. Hoecke, T. Naessens, V. K. Udhayakumar, M. Smet, N. Sanders, S. Lienenklaus, X. Saelens, S. Weiss, G. Vanham, J. Grooten, S.D. Koker, Type I Interferons interfere with the capacity of mRNA Lipoplex vaccines to elicit Cytolytic T cell responses, Mol. Ther. 24 (2016) 2012–2020, https://doi.org/10.1038/mt.2016.161.
[51] M.F. Bachmann, G.T. Jennings, Vaccine delivery: a matter of size, geometry, kinetics and molecular patterns, Nat. Rev. Immunol. 10 (2010) 787–796, https://doi.org/10.1038/nri2868.
[52] T.G. Dacoba, A. Olivera, D. Torres, J. Crecente-Campo, M.J. Alonso, Modulating the immune system through nanotechnology, Semin. Immunol. 34 (2017) 78–102, https://doi.org/10.1016/j.smim.2017.09.007.
[53] A. Schudel, D.M. Francis, S.N. Thomas, Material design for lymph node drug delivery, Nat. Rev. Mater. 4 (2019) 415–428, https://doi.org/10.1038/s41578-019-0110-7.
[54] M.G. Carstens, M.G.M. Camps, M. Henriksen-Lacey, K. Franken, T.H.M. Ottenhoff, Y. Perrie, J.A. Bouwstra, F. Ossendorp, W. Jiskoot, Effect of vesicle size on tissue localization and immunogenicity of liposomal DNA vaccines, Vaccine. 29 (2011) 4761–4770, https://doi.org/10.1016/j.vaccine.2011.04.081.
[55] V. Manolova, A. Flace, M. Bauer, K. Schwarz, P. Saudan, M.F. Bachmann, Nanoparticles target distinct dendritic cell populations according to their size, Eur. J. Immunol. 38 (2008) 1404–1413, https://doi.org/10.1002/eji.200737984.
[56] L. Zhao, A. Seth, N. Wibowo, C.-X. Zhao, N. Mitter, C. Yu, A.P.J. Middelberg, Nanoparticle vaccines, Vaccine. 32 (2014) 327–337, https://doi.org/10.1016/j.vaccine.2013.11.069.
[57] N.M. Belliveau, J. Huft, P.J. Lin, S. Chen, A.K. Leung, T.J. Leaver, A.W. Wild, J. B. Lee, R.J. Taylor, Y.K. Tam, C.L. Hansen, P.R. Cullis, Microfluidic synthesis of highly potent limit-size lipid nanoparticles for in vivo delivery of siRNA, Mol. Ther. Nucleic Acids. 1 (2012), e37, https://doi.org/10.1038/mtna.2012.28.
[58] S. Chen, Y.Y.C. Tam, P.J.C. Lin, A.K.K. Leung, Y.K. Tam, P.R. Cullis, Development of lipid nanoparticle formulations of siRNA for hepatocyte gene silencing following subcutaneous administration, J. Control. Release 196 (2014) 106–112, https://doi.org/10.1016/j.jconrel.2014.09.025.
[59] C. Oussoren, J. Zuidema, D.J.A. Crommelin, G. Storm, Lymphatic uptake and biodistribution of liposomes after subcutaneous injection. II. Influence of liposomal size, lipid composition and lipid dose, Biochim. Et Biophys. Acta Bba - Biomembr. 1328 (1997) 261–272, https://doi.org/10.1016/s0005-2736(97)00122-3.
[60] C. Oussoren, G. Storm, Liposomes to target the lymphatics by subcutaneous administration, Adv. Drug Deliv. Rev. 50 (2001) 143–156, https://doi.org/10.1016/s0169-409x(01)00154-5.
[61] G. Ott, G.L. Barchfeld, G.V. Nest, Enhancement of humoral response against human influenza vaccine with the simple submicron oil/water emulsion adjuvant MF59, Vaccine. 13 (1995) 1557–1562, https://doi.org/10.1016/0264-410x(95)00089-j.
[62] The ICTV, Report on Virus Classification and Taxon Nomenclature, International Committee on Taxonomy of Viruses. https://talk.ictvonline.org/ictv-reports/ictv_online_report/introduction/w/introduction-to-the-ictv-online-report, 2020.
[63] E.J. Lefkowitz, D.M. Dempsey, R.C. Hendrickson, R.J. Orton, S.G. Siddell, D. B. Smith, Virus taxonomy: the database of the International Committee on Taxonomy of Viruses (ICTV), Nucleic Acids Res. 46 (2017), gkx932, https://doi.org/10.1093/nar/gkx932.
[64] Y.M. Bar-On, A. Flamholz, R. Phillips, R. Milo, SARS-CoV-2 (COVID-19) by the numbers, Elife. 9 (2020), e57309, https://doi.org/10.7554/elife.57309.
[65] C.J. Burrell, C.R. Howard, F.A. Murphy, Fenner and White's medical virology (fifth edition), Part II Specif Virus Dis Humans. (2017) 355–365, https://doi.org/10.1016/b978-0-12-375156-0.00025-4.
[66] G.A.C.B. Arbeitskreis B. Blood' Subgroup, Assessment of pathogens transmissible by, human immunodeficiency Virus (HIV), Transfus. Med. Hemother. 43 (2016) 203–222, https://doi.org/10.1159/000445852.
[67] H. Hillaireau, P. Couvreur, Nanocarriers' entry into the cell: relevance to drug delivery, Cell. Mol. Life Sci. 66 (2009) 2873–2896, https://doi.org/10.1007/s00018-009-0053-z.
[68] M. Marsh, A. Helenius, Virus entry: open sesame, Cell. 124 (2006) 729–740, https://doi.org/10.1016/j.cell.2006.02.007.
[69] G. Sahay, D.Y. Alakhova, A.V. Kabanov, Endocytosis of nanomedicines, J. Control. Release 145 (2010) 182–195, https://doi.org/10.1016/j.jconrel.2010.01.036.
[70] A. Aderem, D.M. Underhill, Mechanisms of phagocytosis in macrophages, Annu. Rev. Immunol. 17 (1999) 593–623, https://doi.org/10.1146/annurev.immunol.17.1.593.
[71] D. Paul, S. Achouri, Y.-Z. Yoon, J. Herre, C.E. Bryant, P. Cicuta, Phagocytosis dynamics depends on target shape, Biophys. J. 105 (2013) 1143–1150, https://doi.org/10.1016/j.bpj.2013.07.036.
[72] D.K. Cureton, R.H. Massol, S. Saffarian, T.L. Kirchhausen, S.P.J. Whelan, Vesicular stomatitis virus enters cells through vesicles incompletely coated with Clathrin that depend upon actin for internalization, PLoS Pathog. 5 (2009), e1000394, https://doi.org/10.1371/journal.ppat.1000394.
[73] M.J. Rust, M. Lakadamyali, F. Zhang, X. Zhuang, Assembly of endocytic machinery around individual influenza viruses during viral entry, Nat. Struct. Mol. Biol. 11 (2004) 567–573, https://doi.org/10.1038/nsmb769.
[74] M. Wu, H. Guo, L. Liu, Y. Liu, L. Xie, Size-dependent cellular uptake and localization profiles of silver nanoparticles, Int. J. Nanomedicine 14 (2019) 4247–4259, https://doi.org/10.2147/ijn.s201107.